2007

Observations of a noctilucent cloud above Logan, Utah (41.7°N, 111.8°W) in 1995

J P. Herron

Vincent B. Wickwar
Utah State University

P J. Espy

J W. Merriwether

Recommended Citation
Herron, J. P., V. B. Wickwar, P. J. Espy, and J. W. Meriwether (2007), Observations of a noctilucent cloud above Logan, Utah (41.7°N, 111.8°W) in 1995, J. Geophys. Res., 112, D19203, doi:10.1029/2006JD007158.

Observations of a noctilucent cloud above Logan, Utah (41.7°N, 111.8°W) in 1995

Joshua P. Herron,[1] Vincent B. Wickwar,[1] Patrick J. Espy,[2] and John W. Meriwether[3]

Received 2 February 2006; revised 27 December 2006; accepted 19 February 2007; published 11 October 2007.

[1] A Rayleigh-scatter lidar has been operated at the Atmospheric Lidar Observatory (ALO) on the Utah State University (USU) campus (41.7°N, 111.8°W) since August 1993. During the morning of 22 June 1995, lidar returns from a noctilucent cloud (NLC) were observed for approximately 1 hr, well away from the twilight periods when NLCs are visible. This detection of an NLC at this latitude shows that the first reported sighting, in 1999 (Wickwar et al., 2002), was not a unique occurrence. This 1995 observation differs from the 1999 one in that temperatures could be deduced. Near the 83-km NLC altitude the temperatures were found to be up to ~23 K cooler than the 11-year June climatology for ALO. This analysis shows that these cool temperatures arose, not because the whole profile was cooler, but because of a major temperature oscillation or wave with a 22-km vertical wavelength and a ~0.9 km/hr downward phase speed. This large-amplitude wave has many of the characteristics of the diurnal tide. However, the amplitude would have to be enhanced considerably. These lidar observations were supplemented by OH rotational temperature observations from approximately 87 km. These NLC observations equatorward of 50° have been suggested to be significant harbingers of global change. However, if that were the case, the mechanism is more complicated than a simple overall cooling or an increase in water vapor. Accordingly, we propose enhanced generation of gravity waves that would interact with the diurnal tide to produce a large-amplitude wave, the cold phase of which would give rise to low enough temperatures to produce the NLC. The gravity wave source might be orographic in the Mountain West or convective far to the east or south.

Citation: Herron, J. P., V. B. Wickwar, P. J. Espy, and J. W. Meriwether (2007), Observations of a noctilucent cloud above Logan, Utah (41.7°N, 111.8°W) in 1995, *J. Geophys. Res.*, *112*, D19203, doi:10.1029/2006JD007158.

1. Introduction

[2] Noctilucent clouds (NLCs) typically occur during the summer months between 80 and 86 km in the polar regions or, more specifically, at latitudes greater than 50° [*Gadsden and Schroder*, 1989; *Thomas and Olivero*, 1989; *Chu et al.*, 2003]. They most likely consist of ice particles [*von Cossart et al.*, 1999; *Hervig et al.*, 2001]. NLC observations are important as they may serve as tracers of global change [*Thomas*, 2003]. Lidar observations of NLCs provide information about their altitude, thickness, and magnitude and about the variability of these parameters. The first reported lidar observation of an NLC below 50° was by the ALO lidar group in 1999 [*Wickwar et al.*, 2002]. Because of the possibility that other NLCs might have been observed, but not previously identified, the entire ALO database was searched. A second event was found on 22 June 1995, 4 years earlier than the first reported event.

[3] The lidar and a Michelson Interferometer (Fourier transform spectrometer) are described in section 2 along with their basic data reduction. The 1995 lidar observations, the special data analysis procedures, and their results are given in section 3. The NLC results are discussed in section 4, and the conclusions from the observations and discussion are presented in section 5.

2. Instrument Descriptions and Data Reduction

[4] The Rayleigh-scatter lidar at ALO is located in Logan, UT (41.7°N, 111.8°W) on the Utah State University (USU) campus, 1.46 km above sea level. It has been operated as much as possible since August 1993, giving rise to an extensive database of nighttime mesospheric profiles of relative densities and absolute temperatures.

[5] The lidar is a coaxial system that had a power-aperture product of 3.3 Wm^2 in 1995. The system is composed of a Spectra Physics Nd:YAG laser operating at 30 Hz generating 20–22 watts at 532 nm and having a 44-cm diameter Newtonian telescope. The signals from below ~18 km are blocked by a mechanical chopper and the gain is reduced by almost 1000 by an electronic gate

[1]Center for Atmospheric and Space Sciences, Utah State University, Logan, Utah, USA.
[2]Physical Science Division, British Antarctic Survey, Cambridge, UK.
[3]Department of Physics and Astronomy, Clemson University, Clemson, South Carolina, USA.

0148-0227/07/2006JD007158

for altitudes below 38 km, leading to good data above 41 km. A narrow-band interference filter (1 nm) is used to remove most of the background light from stars, moon, and scattered city lights. The single, gated detector is a green-sensitive, bialkali photomultiplier tube (Electron Tubes 9954B) in a Peltier-cooled housing. A more extensive description of this system is given by *Wickwar et al.* [2001] and *Herron* [2004].

[6] The observations were made in the zenith with an altitude resolution of 37.5 m (250-ns sampling interval) and a temporal resolution of 2 min (3600 laser pulses). In the usual data reduction, the data are averaged over 3 km and 1 hr prior to determining relative densities and temperatures. When the signal from the background light and thermionic emission, determined near 130–180 km, is subtracted from the observed signal and the difference is multiplied by the square of the range, the result is usually proportional to the molecular number density. However, the exception, discussed in the next section, occurs when an NLC is present and added signal is generated by Mie scattering from ice crystals. Temperatures are determined from the relative number densities by using hydrostatic equilibrium and the ideal gas law. The details, as applied to this lidar, are reviewed by *Herron* [2004] and J. P. Herron and V. B. Wickwar (Rayleigh-scatter temperature climatology above the Atmospheric Lidar Observatory (ALO), Logan, Utah, manuscript in preparation, 2007, hereinafter referred to as J. P. Herron and V. B. Wickwar, manuscript in preparation, 2007). However, this data reduction procedure had to be modified to find temperatures in the presence of the NLC. This special analysis is described in the next section.

[7] Temperature data were also available for June 1995 and June 1996 from a Michelson Interferometer that was located approximately 100 m from the lidar and also observing in the zenith. Temperatures were derived at roughly 10-min intervals from the rotational structure of the OH(3,1) Meinel band [*Espy and Stegman*, 2002]. They apply to approximately 87 km, the altitude of the centroid of the OH airglow emission layer [*von Zahn et al.*, 1987; *Baker and Stair*, 1988; *She and Lowe*, 1998], although WINDII observations frequently show the layer peak anywhere between 85 and 90 km [*Liu and Shepherd*, 2006]. The precision of the individual temperature determinations is, on average, 3%, and a minimum of ten measurements are used to determine a nightly average. Unfortunately, because of uncertainties in the OH transition probabilities [e.g., *Burns et al.*, 2003], the OH rotational temperatures cannot be compared directly to the kinetic temperatures from the lidar. However, temporal variations in the OH temperatures are reliable.

3. Observations and Data Analysis

[8] During the early morning hours of 22 June 1995 the lidar was operated from 6:30 UT (00:30 Mountain Daylight Time, MDT) until 10:56 UT (04:56 MDT). An enhancement in the photocount profile above what was expected from Rayleigh scatter alone was observed in 2-min profiles between 8:03 and 8:54 UT (from the beginning of the first 2-min observation to the end of the last 2-min observation) and more weakly between 9:39 and 9:48 UT. It is presumed that these enhancemen se from Mie scatter from an

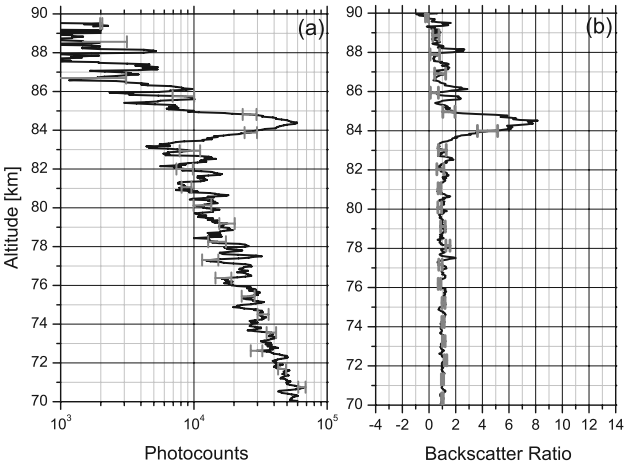

Figure 1. The NLC enhancement on 22 June 1995 at ALO seen in the profiles of relative density Figure 1a and the backscatter ratio Figure 1b. The data were averaged over 12 min, centered on 8:13 UT, and over 150 m. However, data points are plotted every 37.5 m. The uncertainties are based on the measurements, assuming Poisson statistics.

NLC. These time periods with the Mie scatter correspond to solar depression angles between 17.3° and 24.3° for which the shadow heights are between ~300 and ~600 km, well above the observed Mie scatter enhancements. Accordingly, the NLC, at altitudes below 85 km, was in the Earth's shadow and could not have been observed visually from the ground. Nonetheless, we still take the liberty of calling it an "NLC".

[9] The lidar raw photocount profiles typically include contributions from background light and photomultiplier-tube dark count as well as from Rayleigh backscatter, which is proportional to atmospheric number density. When an NLC is present, there is an additional contribution from Mie scatter from the large particles that make up the NLC, which is seen as an enhancement in the photocount profile. When the background light and dark count are subtracted from this profile and the values are multiplied by range squared, this becomes the relative density profile, which is shown in Figure 1a. The signal from the peak of the NLC layer is equivalent to the Rayleigh-scatter density at an altitude of ~70 km.

[10] The backscatter ratio $R(z)$ is commonly used as a measure of the NLC strength. It is the ratio of the measured signal $S(z)$, as contributed to Figure 1a, to the Rayleigh-backscattered signal $S_R(z)$:

$$R(z) = \frac{S(z)}{S_R(z)} = \frac{S_R(z) + S_m(z)}{S_R(z)} \tag{1}$$

where $S_m(z)$ is the Mie-backscattered signal. To reduce the variability, the photocount profiles were smoothed by making running averages in both altitude and time. To minimize distorting the NLC parameters, the averaging was carried out over only 4 points in altitude (150 m) and 6 points in time (12 min). However, the profile for the Rayleigh-scattered signal S_R used to calculate the backscatter ratio R in equation (1) was found by averaging all the periods without evidence of the NLC during the night

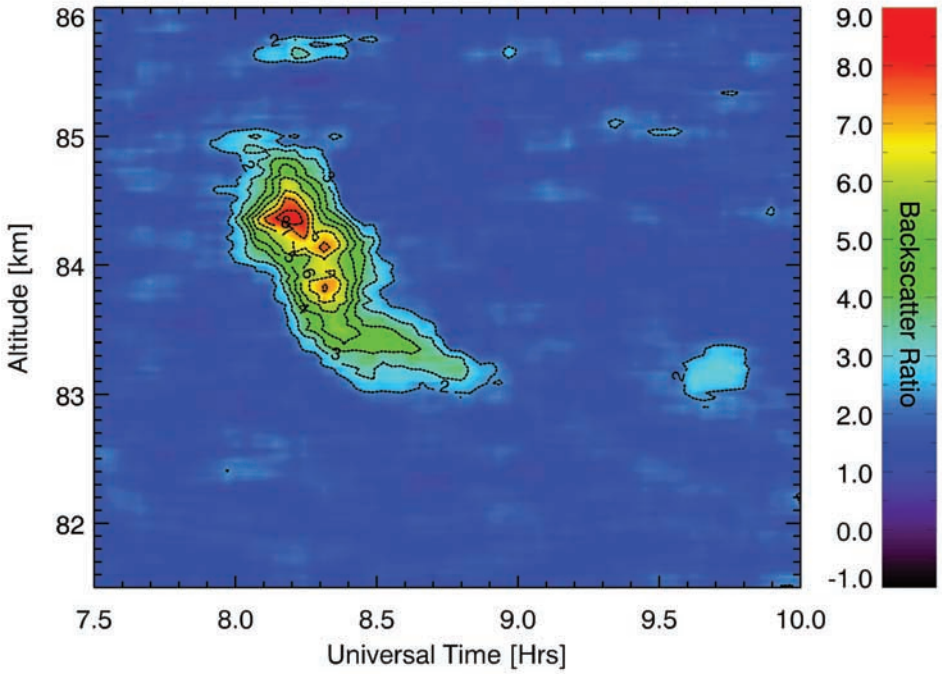

Figure 2. Backscatter ratios for the 22 June 1995 NLC. The inputs for the contour plot were created every 2 min using a two-dimensional running average with a width of 12 min and a height of 150 m applied to the raw data, which were measured every 2 min and every 37.5 m. A backscatter ratio of 1 indicates that there is no Mie-scatter enhancement. The time is in hours.

of 22 June. To further minimize the possibility of contamination by Mie scatter, a third order polynomial was fitted to the average photocount profile, S_R, at 37.5-m intervals from 79 to 82 km and from 85 to 88 km, excluding the region of the NLC. The polynomial was then used to replace the observations between 82 and 85 km. A smoothing function over 41 points, 1.5 km, was then applied to minimize the fluctuations in this Rayleigh profile.

[11] These 12-min profiles of the backscatter ratio were derived every 2 min. From them it was determined that the maximum backscatter ratio for the NLC was 9.6 and it was centered on 8:13 UT. The corresponding profile is shown in Figure 1b. These profiles also were used to create a contour plot of the backscatter ratios (Figure 2). This shows the main body of the NLC between 7:54 and 8:58 UT (from the beginning of the first 12-min observation to the end of the last 12-min observation), and an additional small enhancement in the backscatter ratio between 9:31 and 9:54 UT at ~83.1 km. During the period that the main body of the NLC had a BSR of 2 or more, the NLC descended very slowly from 84.4 to 84.3 km, fairly rapidly to 83.4 km, and then slowly to 83.2 km. Between 8:01 and 8:16 UT, a least squares fit gives a rate of −0.08 m/s, between 8:18 and 8:32 UT a rate of −3.3 m/s, and between 8:34 and 8:51 UT a rate of −0.9 m/s. While several small regions with a BSR of 2 exist in Figure 2, the largest of them is at this lowest altitude, at 83.2 km. Because of its greater extent in altitude and time and its altitude, this was identified as a small NLC enhancement. The other regions are considered to be noise fluctuations.

[12] At the height of the NLC, the diameter of the laser beam is ~40 m, which that only a very small portion of the cloud is sampled at any instant. Furthermore, the beam is fixed in the zenith direction preventing any knowledge of the horizontal extent or structure of the cloud. Accordingly, it is not possible to distinguish between a layer descending in the beam, a slanted layer being transported horizontally across the beam, or a combination of the two. Accordingly, the deduced descent rates are really apparent descent rates.

[13] To compare these NLC observations to those made in 1999 [*Wickwar et al.*, 2002], the results from the 1999 NLC were reanalyzed using the same temporal and spatial averaging as for the 1995 NLC (Figure 3). The 1995 NLC maximum backscatter ratio occurs at a higher altitude, 84.4 versus 82.1 km, and has a greater maximum backscatter ratio. It was 9.6, 90% greater than the maximum of 5.1 reached by the 1999 NLC. This does not mean that the 1995 NLC backscattered 90% more light. Part of this greater backscatter ratio occurs because the Rayleigh contribution to the backscatter ratio [the denominator in Equation (1)] is smaller at the higher altitude. By using the observed relative density profile, the backscatter ratio of 9.6 at 84.4 km translates to 6.7 at 82.1 km, only 31% greater than that of the 1999 observation, assuming the same neutral densities at 82.1 km on both occasions. Thus the biggest difference between the two NLCs is that the one in 1995 was 2.3 km higher.

[14] In addition to these results concerning the NLC altitude, another significant difference occurred between the 1995 and 1999 observations. In 1995 the background signal was well behaved, which is extremely important for deriving temperatures, especially at the highest altitudes (J. P. Herron and V. B. Wickwar, manuscript in preparation,

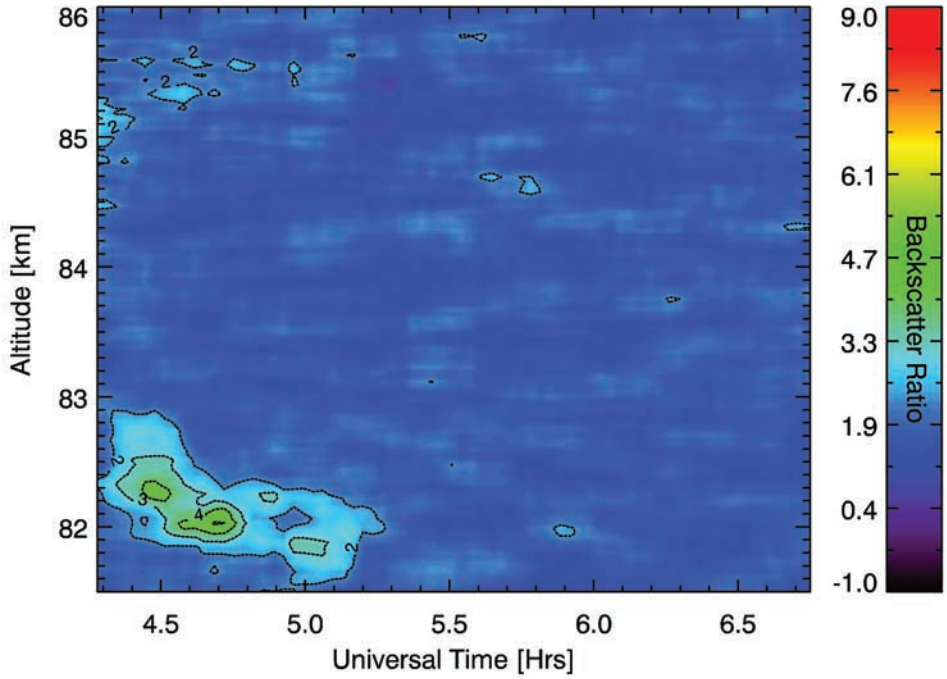

Figure 3. Backscatter ratios for the 1999 NLC [*Wickwar et al.*, 2002] analyzed and presented in the same way as for the 1995 NLC in Figure 2. It is at a lower altitude and the maximum backscatter ratio is smaller.

2007). Furthermore, the laser had more power, which is essential for deriving temperatures above the NLC altitude. This possibility of obtaining temperatures in 1995 provides an important additional dimension to the NLC observations.

[15] To determine density and temperature profiles, the individual 2-min profiles are averaged together during three periods. The first period (06:30–08:00 UT) extends from the start of observations for the night to just prior to the start of the NLC observations. The second (08:00–09:00 UT) encompasses the period when the NLC was observed and extends a little on either end, and the third (09:00–10:56 UT) spans the time from just after the NLC to shortly before dawn. The first period has no discernable NLC enhancement and was used to examine fitting routines for interpolating across the NLC. Several low-order polynomials were fitted over the same region used in calculating the backscatter ratio, but with independent points every 37.5 m. A third order polynomial fitted to the density profiles, excluding the 82- to 85-km region of the NLC, produced a reasonable fit and higher orders did not significantly improve the χ^2 values. Similarly derived fits were used to interpolate across the NLC region for all three time periods to remove any effects from Mie scatter. These curves were then smoothed in altitude with a running average over 81 points (3 km). The first two relative density profiles are shown in Figures 4a and 4b. The wide black curves are the observed relative density. The narrow gray curves are the combination of the observations and the fits. In Figure 4a the gray and black curves are almost indistinguishable, whereas in Figure 4b the gray curve smoothly bridges the region under the black NLC curve. (Because of the 3-km smoothing, the altitude gap bridged by the fit appears to be greater than the actual 3-km gap.) The fitted profiles are then used to calculate the corresponding temperature profiles, which are shown in Figure 5.

[16] To our knowledge, this is the first time Rayleigh-scatter temperatures have been derived in the presence of an

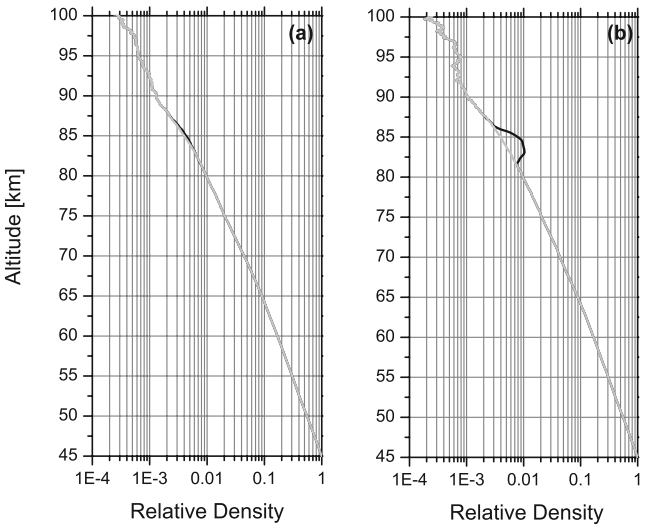

Figure 4. Relative density profiles before Figure 4a and during the NLC Figure 4b. The thick black curves are the measured number density profiles; the thin gray curves are the result of a third order polynomial fitted to data in 3-km regions immediately above and below the NLC and then applied across the 3-km region in between. A 3-km running average was applied to both the measured number density profile and the profile with the polynomial fit. See the text for details about the fitting procedure.

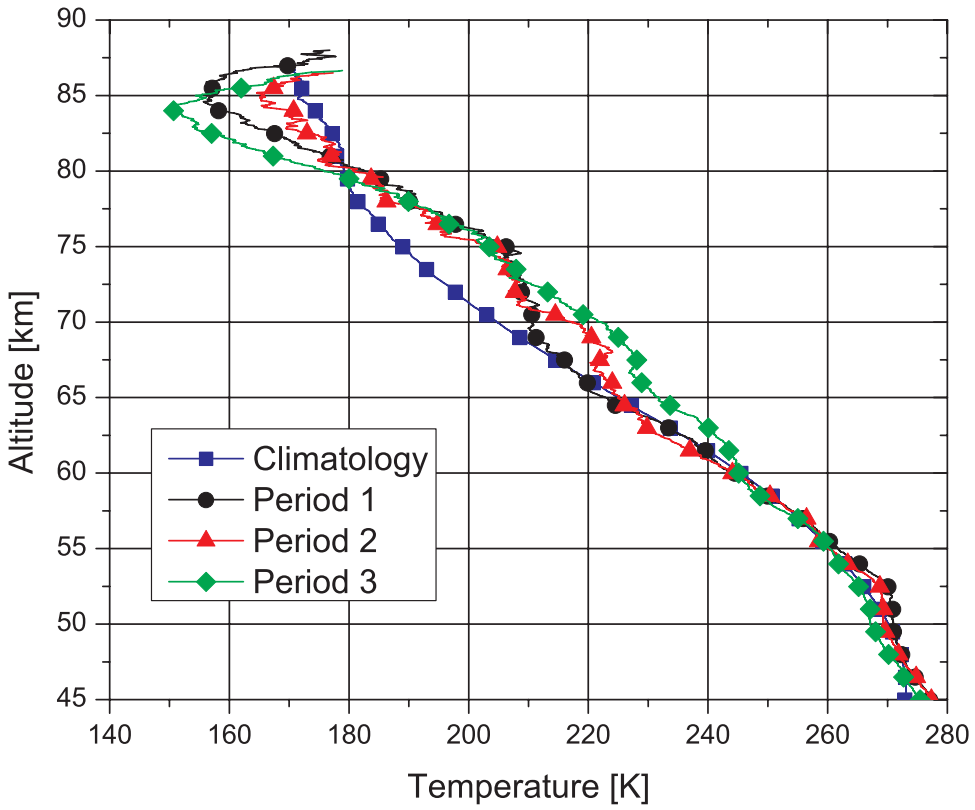

Figure 5. Temperature profiles before, during, and after the NLC on 22 June 1995. Period 1 is for 6:30–8:00 UT, period 2 for 8:00–9:00 UT, and period 3 for 9:00–10:56. The fourth profile is the average June temperature from the ALO climatology (J. P. Herron and V. B. Wickwar, manuscript in preparation, 2007). The corresponding density profiles for periods 1 and 2, from which the temperatures were derived, are shown in Figure 4.

NLC. However, steps in this direction have been taken by others. *Collins et al.* [2003] interpolated across the NLC layer to calculate the backscatter ratio, but only calculated temperatures below the NLC layer. *Lübken et al.* [1996] interpolated lidar measurements across the NLC region to find the molecular signal for calculating the backscatter ratio when additional density measurements were not available from falling spheres. *Stebel et al.* [2004] interpolated across a possible wintertime aerosol layer at lower altitudes to calculate Rayleigh temperatures.

[17] To derive absolute temperatures from the relative density profiles, a "best guess" temperature is needed at the highest altitude. The highest altitude, in this analysis, is determined to be the point where the signal has dropped to 20 times its one standard-deviation uncertainty. The "best guess" value was taken from the temperature climatology from the Colorado State University (CSU) sodium lidar [*She et al.*, 2000]. While this is a climatological value, it is still the best source available for a particular night. The temperature profiles for the three periods are shown in Figure 5 along with the 11-year, June climatological average for ALO (J. P. Herron and V. B. Wickwar, manuscript in preparation, 2007). The temperature uncertainties are from a full error propagation starting from the observed photocounts [*Gardner*, 1989; *Herron*, 2004], assuming Poisson statistics. The total variability, measurement plus geophysical, for an individual ni ht in the 11-year average is not shown, but is found to be, for example, 12 K at 84 km, 8.4 K at 71.5 km, and 3.7 K at 60 km. It is derived using the 103 nighttime June temperatures and their mean to calculate the standard deviation (J. P. Herron and V. B. Wickwar, manuscript in preparation, 2007). The total variability, then, for the mean June profile is 10% of those values.

[18] The minimum temperatures for the three 22 June profiles are found near 84 km and are considerably colder than for the June climatological average. The differences between these temperature profiles and the climatological average are presented in Figure 6. The first and third profiles reached minimum values between 150 and 160 K in this region and became 17–23 K cooler than the average. The second period was slightly warmer. In contrast, centered on 73 km, all three temperature profiles became significantly warmer by ~17 K than the climatological average. The negative and positive departures from the June average clearly have the appearance of a large vertical temperature oscillation or wave.

[19] The properties of this wave were examined directly by overlaying profiles and by both autocorrelation and cross correlation of the profiles. The altitudes of the temperature minima occur between 85 and 83 km and of the maxima between 74 and 72 km. The best value for the vertical wavelength is ~22 km. The deduced phase velocity is highly variable. The average value for the three profiles varies from −0.6 to −0.8 km/hr depending on how it is

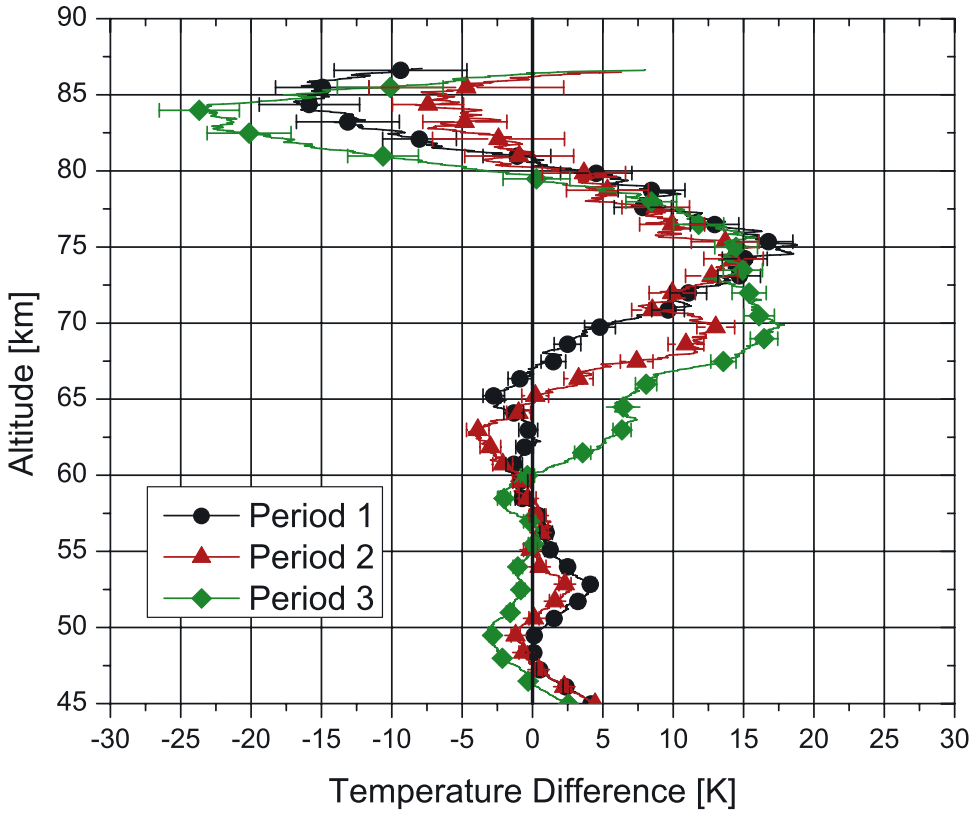

Figure 6. Temperature differences between the observed values on 22 June 1995 and the climatological June average for ALO. The temperature profiles are from Figure 5.

derived. Overlaying small portions of one temperature profile over another gives the best results. The minimum near 84 km has a relatively constant phase velocity of −0.6 km/hr and the maximum near 73 km has phase velocities that vary from −1.8 km/hr between periods 1 and 2 to −0.3 km/hr between periods 2 and 3, with a value of −0.9 km/hr between periods 1 and 3, which encompasses the NLC. The uncertainties are less than 0.2 km/hr. Part of these changes in the apparent phase velocity probably occurs because the shape of the maximum is changing with time. It is becoming thicker.

[20] To provide context for the NLC observations, additional temperature measurements would be desirable. Unfortunately, very few good lidar observations exist in June 1995 and 1996. In 1995, the observations preceding the 22nd were plagued by cloud cover. On the following two nights the lidar was operated for a minimum of 6 hr providing reasonable temperature profiles. The all-night temperature profile from the 23rd is similar to the three profiles from the 22nd with a wave and a temperature minimum between 150 and 160 K. On the 24th the temperature minimum is at 81 km; however, it has no discernable positive departure from the June average near 73 km. The lidar was not operated in June 1996.

[21] However, as discussed in the previous section, a Michelson Interferometer was operated at USU during June 1995 and 1996. Temperatures from these observations, nominally from 87 km [*Baker and Stair*, 1988], are shown in Figure 7. It is apparent that the all-night temperatures from 19 to 24 June 19 particularly cool and that the temperature for 22 June 1995 is significantly cooler than for all the other nights. In addition, the June 1995 nights are systematically cooler than the June 1996 nights by an average of 16 K. While this is a large amount, it is plausible when compared to the observed standard deviations for June in the ALO climatology (J. P. Herron and V. B. Wickwar,

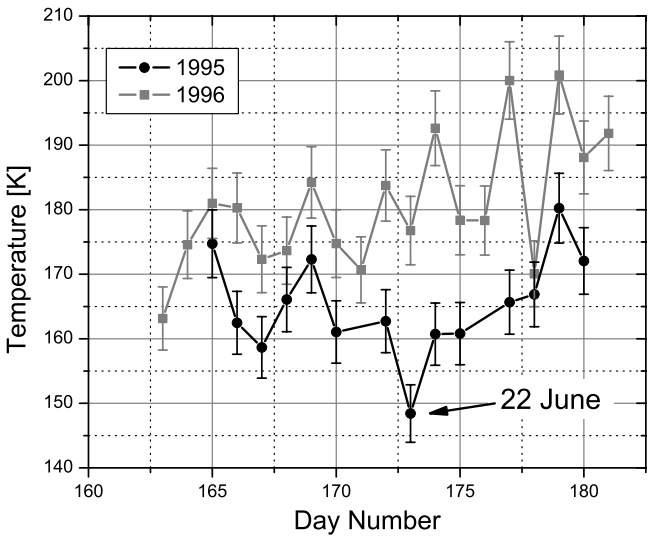

Figure 7. Nighttime OH rotational temperatures at ~87 km from the Michelson Interferometer located at USU. The squares denote the values from 1995; the circles denote those from 1996. The NLC night is identified.

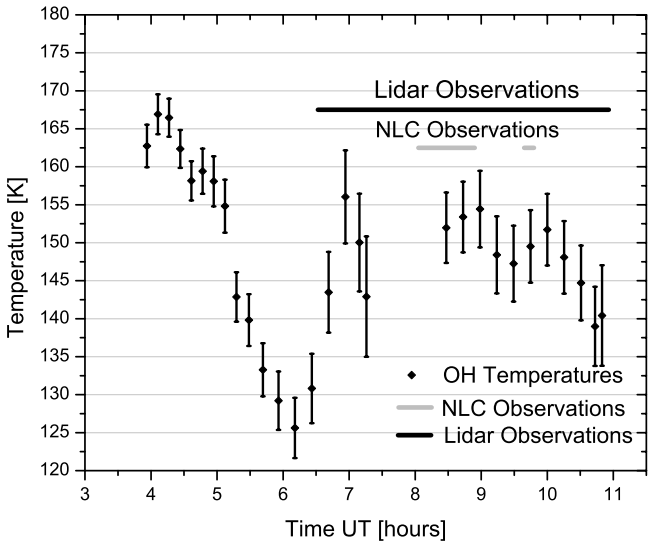

Figure 8. OH rotational temperatures at ~87 km for the night of 22 June 1995. In addition, the time period when the lidar was operated is indicated in black and when the NLC was observed is indicated in gray.

manuscript in preparation, 2007). That standard deviation contains the combined effects of day-to-day variability, interannual variability, and long-term trends. At 84 km, the highest altitude for which it was tabulated, the standard deviation is 12 K. That value is an underestimate because 84 km is close to the altitudes for which the initial values were found. A better estimate of the standard deviation can be found by extrapolating the values found at lower altitudes, far removed from the initial values. A linear extrapolation of the standard deviations from 66 to 75 km gives a value of 14 K at 84 km and 16 K at 87 km. That the 13 nights in 1996 are all warmer than the corresponding nights in 1995 suggests that this difference arises from an interannual variation. Whether considering the 1995 data alone or in combination with the 1996 data, it is apparent that 22 June 1995 is an unusually cold night at 87 km.

[22] Temperatures from the Michelson Interferometer are also available at subhour intervals, as shown for 22 June 1995 in Figure 8. The temperatures dropped quickly after 05:00 UT to a minimum at 06:11 UT and then returned to a level less than the initial one. Compared to this later level, the minimum temperature was ~30 K less. This variation suggests a wave in time with high temperatures initially, followed by low temperatures, which would be consistent with the descent of the type wave seen in the lidar profiles. The amplitude of the cold portion of the wave is greater than deduced for the lidar data. Ignoring holes in the data, the lowest temperatures were observed 1.07 hr before the first lidar temperature profile with its lowest temperature at 84.5 km and 1.84 hr before the appearance of the NLC in the lidar data at 84.4 km.

[23] This large oscillation in time in the OH temperatures is at a slightly higher altitude and prior to the lidar observations of the vertical temperature wave and of the NLC observations. If these are two manifestations of the same wave, then the combined temperature observations indicate that it descends at a rate of 2.3 km/hr assuming the centroid of the OH emi s at 87 km or 1.4 km/hr if it is at 86 km. The time to the appearance of the NLC would indicate a descent rate of 1.4 km/hr for the OH originating from 87 km or 0.9 km/hr for it originating from 86 km.

4. Discussion

4.1. NLC Characteristics

[24] The magnitudes of both the 1995 and 1999 NLCs detected at ALO at 41.7°N are weak compared to those observed at higher latitudes where the backscatter ratio can be greater than 200 [e.g., *Hansen et al.*, 1989; *Langer et al.*, 1995; *Thayer et al.*, 1995; *Fiedler et al.*, 2003]. When adjusted for altitude, the 1995 NLC was about 30% stronger than the 1999 one.

[25] A strong linear trend in NLC altitude versus latitude has been found for NLC events [*von Zahn and Berger*, 2003; *Chu et al.*, 2004]. The 1999 NLC shows a mean altitude of 82.1 km, which is in very good agreement with that linear trend. However, the mean altitude of the 1995 NLC observation was 83.8 km, 1.7 km higher and significantly above the linear trend. Whether this indicates different origins for the two NLCs is more than can be determined from the available data. However, what is clear from the lidar temperatures is that the 1995 NLC is unusual in that it occurs at the minimum of a large-amplitude vertical temperature wave. The main portion of the NLC occurred between 7:54 and 8:58 UT. During that time it descended from 84.4 km to 83.2 km, with its average height at 83.8 km. The minimum in the temperature profile integrated over this period is at 84.0 km.

[26] This wave is the dominant feature in Figure 6. It shows a persistent, large, temperature oscillation or wave with a maximum amplitude of 23 K for the cold phase at 84 km and a maximum amplitude of 17 K for the hot phase at 73 km. The lowest temperature from these three profiles is ~150 K. From the minima and maxima in this wave, the inferred vertical wavelength is 22 km. In addition to the lidar data, a time series of OH temperatures from a Michelson Interferometer from ~87 km shows a large oscillation in time with a temperature minimum ~30 K below the subsequent temperatures at ~125 K. The temperature minimum occurs a little more than an hour prior to the beginning of the lidar observations and a little less than 2 hr prior to the NLC detection. Combining the Michelson and lidar observations, assuming the OH emission is centered at 87 km, leads to descent rates of −2.3 km/hr and −1.4 km/hr for these two intervals. However, if the OH emission were centered at 86 km, well within the range of uncertainty and variability, the descent rates become −1.4 km/hr and −0.9 km/hr. The lidar results for these three integrations show a nearly constant descent rate of −0.6 km/hr for the temperature minima near 84 km between 06:30 and 10:56 UT (start and end times for the lidar data). In contrast, the temperature maxima, from ~11 km lower, show a rate that decreases with time from −1.7 km/hr between periods 1 and 2 to −0.3 km/hr between periods 2 and 3. Between periods 1 and 3, it has the average value of −0.9 km/hr. While the descent rate deduced from the minima is much slower than the two inferred values from the OH observations, the rate from the earliest two lidar periods for the maxima is consistent with the OH observations. Furthermore, while the minima

appear to have a constant descent rate, the maxima show a descent rate that is slowing with time, which is consistent with what is inferred from the OH observations. If the minima and maxima are descending at the same rate, the wavelength should be constant, whereas if they are descending at different rates, the wavelength should vary. However, the amount is less than the 1-km precision of the wavelength determinations. Combining these observations concerning the descent rates, it appears that the altitude and magnitude of the temperature minima may be influenced by being close to the initial temperature. Because the initial temperature is based on climatological values it is probably higher than it should be for this particular day. The impact of this is that the temperature minimum would be either at a lower altitude than it should be or would not extend over as large an altitude region as it otherwise would, and that the minimum would have a higher temperature than it should have. Two other implications are that the layer would not appear to move downward as quickly as it should and that as it did move downward the minimum temperature would decrease. The point of this discussion is that the descent speed of the minimum may be closer to that of the maximum than what was actually measured. In that case, it would be very similar to the value of -0.9 km/hr inferred by combining the OH and lidar measurements. This supports the idea that these two instruments are detecting different manifestations of the same wave.

[27] As for NLCs being associated with temperature minima of large vertical waves, this observation appears to be a first. Previously, large waves with amplitudes of 20 K, similar to this wave, have been reported at high latitudes at NLC altitudes by *von Zahn and Meyer* [1989], but not in conjunction with an NLC.

[28] Temperatures at high latitudes, derived from falling spheres released from rockets, have shown that NLCs typically occur when the temperature is 150 K or lower [*Thomas*, 1991; *Lübken et al.*, 1996; *Lübken*, 1999]. While, the June temperature climatology for ALO gives a much higher temperature, $\sim$173 K, on average at the NLC altitude of 84 km, the wave observations for 22 June 1995 show the temperature at 84 km reaching the immediate vicinity of 150 K. The Michelson Interferometer temperatures even reach the vicinity of 125 K at $\sim$87 km.

[29] Combining the two sets of temperature results and the NLC results, it appears that the wave caused the temperatures to drop low enough to start forming ice crystals at 87 km or so. The growing particles probably descended initially at the same rate as the wave. However, shortly after they become large enough to backscatter detectable radiation, they became massive enough for sedimentation to occur at a faster rate. For 15 min in the middle of the hour when the NLC was detected, it descended at an apparent rate of -3.3 km/hr. When the cloud reached 83.5 km at 8:30 UT, the backscatter ratio started to decrease significantly and the descent slowed to -0.9 km/hr. The peak BSR was not seen below 83.2 km. Presumably, the ice crystals were sublimating on the bottom side of the NLC. And, given this scenario, it is most likely that the small, detached NLC observed between 9:31 and 9:54 UT at 83.2 km was transported into the lidar field of view.

4.2. Relationship Between the NLC and Climate Change

[30] The appearance of NLCs at latitudes <50°N suggests a manifestation of global climate change [*Thomas*, 1996, 1997, 2003]. These predictions follow from model calculations based on large increases in greenhouse gases and methane leading, respectively, to a cooling in the upper mesosphere and an increase in water vapor concentration that would increase the temperature at which water vapor freezes spontaneously. However, NLCs were observed at 41.7°N at ALO in June 1995 and 1999, much sooner than predicted for the large increases in these gases to have occurred. And indeed, it is a period when the ALO temperature climatology shown in Figure 5 (J. P. Herron and V. B. Wickwar, manuscript in preparation, 2007) does not show evidence of such significant cooling. Nor is there evidence of a strong increase in water vapor. Among the few observations of mesospheric water vapor, *Chandra et al.* [1997] and *Nedoluha et al.* [2003] show an inverse correlation with the variation of Lyman α during the solar cycle. This would give a small maximum in water vapor concentration in the summer of 1995, but not in 1999. If increased water vapor were the explanation in 1995, a different explanation would be needed for 1999. While possible, this seems unlikely. Trend information for water vapor is not particularly clear, but appears to be considerably less than the solar cycle effect. As for episodic events, the closest Shuttle launch, which might have injected water vapor into the mesosphere, was almost 4 months prior to this noctilucent cloud detection, 2 March 1995. Thus it is unlikely that either mesospheric cooling or increased water vapor could account for this NLC.

[31] It may be noteworthy that this second NLC found equatorward of 50° latitude was also found at ALO and not at one of the other Rayleigh-scatter or Na lidars operating at midlatitudes. This raises the question as to whether there could be a longitudinal effect associated with the Mountain West where ALO is located. Such an effect might arise from orographically generated gravity waves, nonmigrating tides, or stationary planetary waves over this extremely mountainous region. This is consistent with a suggestion made to account for NLC formation at higher latitudes over the Rockies [*Espy et al.*, 1995].

[32] Furthermore, this second NLC observation at ALO confirms that NLCs are occurring at lower latitudes than previously. If their occurrence is related to global change, as opposed to better observations, then the generation of the wave associated with the NLC observed in 1995 would have to be a manifestation of that change. The generation of the wave would, needless to say, have to be from a more complicated mechanism than uniform mesospheric cooling. As suggested above, a mechanism might involve the interaction of winds with the topography of the Mountain West to generate gravity and mountain waves or to contribute to nonmigrating tides or stationary planetary waves. If it has to do with gravity waves, they might interact with the diurnal tide, as discussed next, to enhance the tidal amplitude. In either case, more or stronger tropospheric winds would be needed.

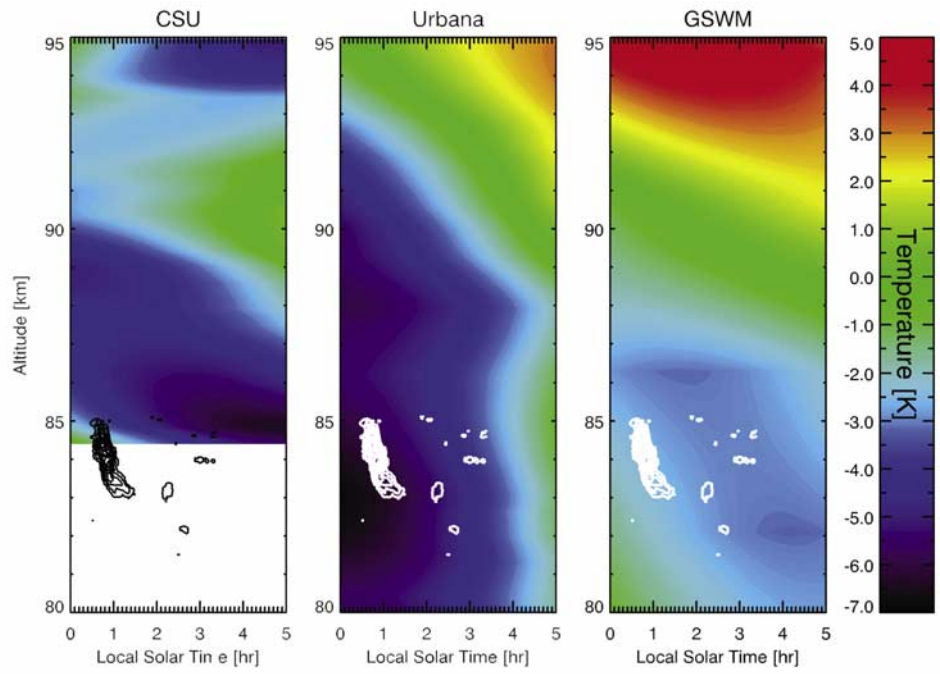

Figure 9. Amplitude and phase of the diurnal tide compared to the NLC. The tidal results were derived from the CSU sodium lidar measurements [*She et al.*, 2002], Urbana sodium lidar measurements [*States and Gardner*, 2000], and GSWM-00 model calculations [*Hagan et al.*, 1999, 2001]. Local solar midnight corresponds to 7:27 UT.

4.3. Comparison of Large Amplitude Waves and Tides

[33] A potential seed for the observed wave might be an atmospheric tide. What is known about the diurnal and semidiurnal tides in this region can be compared to the observed NLC and the large-amplitude wave. Figure 9 shows contours of the June 1995 NLC (actually, all regions with a BSR ≥ 2) superimposed on the summer temperature structure from the diurnal tide derived from the midlatitude sodium lidars at CSU (41°N) and Urbana (40.2°N) [*She et al.*, 2002; *States and Gardner*, 2000] and the Global Scale Wave Model for 2000, GSWM-00, calculations for June at 42°N latitude [*Hagan et al.*, 1999; *Hagan et al.*, 2001]. Figure 10 is similar to Figure 9, but it shows contours of the June 1995 NLC superimposed on the temperature structure from the semidiurnal tide derived from observations at CSU and Urbana and calculated for GSWM-00. (The GSWM amplitudes have been multiplied by 10.) For the diurnal tide, the main body of the NLC is close in altitude and time to the temperature minima. For the semidiurnal tide, the main body of the NLC is close to the zero amplitude point for GSWM and probably for CSU, but it is close to the temperature maximum for Urbana. These comparisons show the NLC and the ALO temperature minimum to be much more consistent with the phase of the diurnal tide than with the semidiurnal tide.

[34] Additional comparisons can be made with other tidal parameters. Concentrating on the diurnal tide, vertical wavelengths can be compared. The vertical wavelength of the observed wave at ALO is ~22 km. For this to be related to a diurnal tide, the phase velocity would be −0.9 km/hr, which agrees well with the deduced phase velocity, showing great internal consiste he diurnal component of the CSU temperatures [*She et al.*, 2002] gives a descent rate of ~−0.8 km/hr, which corresponds to a vertical wavelength of ~20 km. For GSWM it is ~−1.3 km/hr, giving a vertical wavelength of ~32 km. For Urbana it is also ~−1.3 km/hr above 88 km, but becoming indeterminate below that. Thus the ALO observations are in very close agreement to the CSU diurnal tidal observations. They are about 70% of the values found for GSWM and for Urbana.

[35] Turning to the semidiurnal tide, if the ALO descent rate of −0.9 km/hr is applied for 12 hr, it would give rise to a 12-km vertical wavelength instead of the observed 22 km. Thus, by themselves the ALO observations are not consistent with a semidiurnal tide, neither are the other observations and model calculation. Both CSU and GSWM show descent rates of ~−4 km/hr near 84 km, giving rise to a vertical wavelength of ~48 km. Urbana shows a much greater descent rate, which would give rise to an even longer vertical wavelength. These very rapid descent rates and long vertical wavelengths are inconsistent with the observations. Thus if one of these two tides is the seed for the NLC wave, then the diurnal tide is a much better candidate.

[36] While the phase, phase velocity, and vertical wavelength of the diurnal tide are similar to the characteristics of the observed NLC wave, the amplitude of the diurnal tide is far smaller than the amplitude of the wave. The average amplitude of the two observed and one modeled diurnal tidal results is ~4 K at the time of the wave, which has an observed maximum amplitude of 17 K at 73 km growing to 23 K at the minimum at 84 km. However, if the tidal amplitude could be enhanced or amplified, this difference could be accounted for. Several studies have examined the

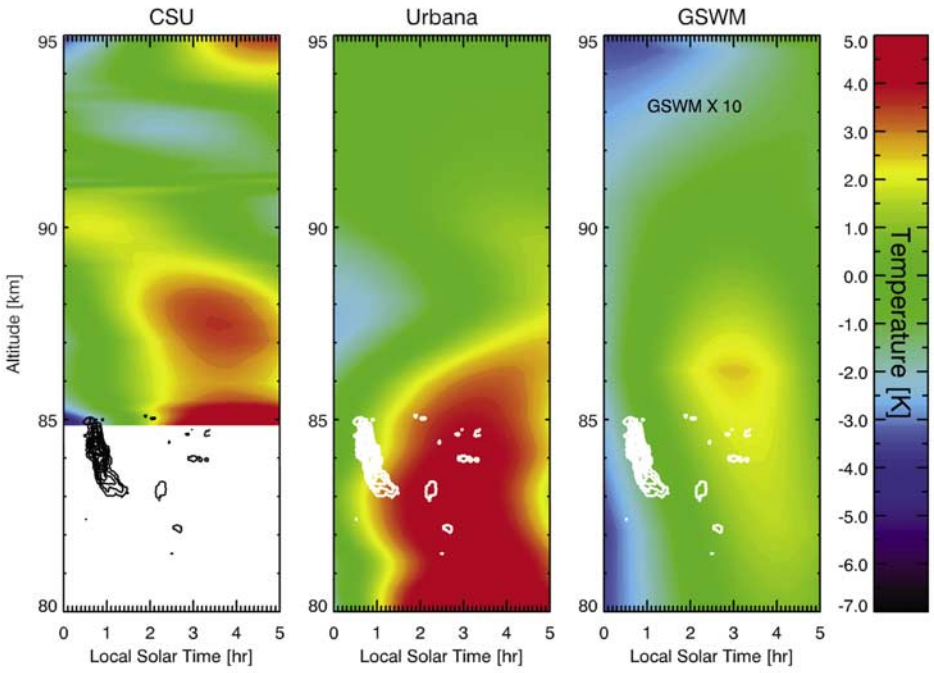

Figure 10. Amplitude and phase of the semidiurnal tides in relation to the NLC occurrence. The tidal results are derived from the CSU sodium lidar measurements [*She et al.*, 2002], Urbana sodium lidar measurements [*States and Gardner*, 2000], and GSWM-00 model calculations [*Hagan et al.*, 1999, 2001]. The model values had to be multiplied by 10 to use the same scale as the two sets of observations. Local solar midnight corresponds to 7:27 UT.

interaction of breaking gravity waves with the mean flow or the diurnal tidal winds. *Walterscheid* [1981] suggests a cooling high in the mesosphere. More recent works [*Liu and Hagan*, 1998; *Liu*, 2000; *Liu et al.*, 2000] have specifically looked at the interaction with tides. While their purpose was to try to explain the temperature enhancements in mesospheric inversion layers, their mechanism may also be very applicable in this situation. Like *Walterscheid* [1981], they produced a cooling at higher altitudes. However, in addition, they produced a warming at lower altitudes. This might account for an enhanced diurnal tide or, in this case, the large-amplitude wave.

[37] Although speculative, this second NLC observation at ALO is consistent with the idea of increased gravity-wave generation in the troposphere in the Mountain West, which leads to a large enhancement of the diurnal tide in the upper mesosphere. The negative or cold portion of this enhanced tide then produces low enough temperatures to enable an NLC to develop. This could be a unique event from unusual local circumstances. Or, if these midlatitude NLCs are truly a recent recurring phenomenon, this could be a manifestation of climate change in the troposphere that is coupled to the mesosphere via gravity waves.

5. Conclusions

[38] Previously, we showed [*Wickwar et al.*, 2002] the first NLC detected by lidar below 50° latitude. Here we present the second NLC detected below 50° latitude. It was observed at the same location at 41.7°N on 22 June 1995, 4 years earlier. This det was found during a systematic reanalysis of the ALO Rayleigh-scatter data searching for NLCs. While no visual observations could have been made, this is definitely another midlatitude NLC: there is an enhanced backscatter ratio, it occurs near summer solstice, it occurs in the usual NLC altitude range, the enhancement is confined to a thin layer, this layer is located at a very low temperature minimum, and the layer descends slowly with time.

[39] To date, this is the second reported lidar observation of an NLC below 50°. It shows that the first observation was not an anomaly and further suggests that additional NLCs could have occurred at mid and lower latitudes, but were not detected. It is somewhat surprising that this second detection was from the same location in the Mountain West.

[40] To our knowledge, the June 1995 observation at ALO is the first time that Rayleigh lidar data have been analyzed for the coincident neutral temperatures. In an unexpected result, this NLC was found at the minimum of a large-amplitude vertical temperature wave. The wave was characterized by a cold phase with an amplitude of ~23 K near 84 km and a warm phase, maximizing 11 km lower, with an amplitude of ~17 K, a vertical wavelength of 22 km, and a deduced downward phase velocity of ~−0.9 km/hr. The apparent wave modulation was probably essential for producing the low temperatures necessary for formation of the NLC ice crystals. The Michelson Interferometer observations suggest that the temperature minimum in the wave may have been further lowered by interannual variability. The phase, phase velocity, and vertical wavelength of this wave suggest that it is an enhanced diurnal tide. Modeling results in the literature, performed for other

reasons, suggest that the diurnal tide could be significantly enhanced by interactions with gravity waves propagating from below.

[41] While the first NLC detection led to speculation about global change having either lowered mesospheric temperatures or increased mesospheric water vapor and its freezing point, the temperatures and the large-amplitude wave in this detection lead to different speculation. Below 60 km or so, the temperatures on 22 June 1995 were close to the climatological mean derived from lidar observations between 1994 and 2004. Above that altitude, the temperatures are dominated by a large-amplitude wave that appears to grow with altitude in both the lidar and Michelson Interferometer results. The climatological temperatures are not cold enough to produce NLCs. Thus, the NLC did not arise from overall mesospheric cooling. It was definitely helped by the large-amplitude wave, which lowered the temperatures to ~150 K at 84 km and ~125 K at ~87 km. These temperatures are typical of the lower temperatures observed at high latitudes at which NLCs are found. Possibly, its formation was also helped by increased water vapor, but we do not have information on that.

[42] The speculation about the origin of the NLC has to turn from a significant mesospheric cooling to the origin of this large-amplitude wave or to the gravity waves that may have caused it by, perhaps, enhancing the diurnal tide. This large-amplitude wave might have been a unique event, although the temperatures on the next day, 23 June 1995, suggest otherwise, or it might be a very different manifestation of global change. If caused by a change in the gravity waves reaching the upper mesosphere, then either the gravity-wave source has to be enhanced or the filtering between the source region and the upper mesosphere has to be reduced. Either of these possibilities suggests changes in wind systems. If large-amplitude mesospheric waves are localized in longitude to the Mountain West, as weakly suggested by the absence of midlatitude NLC observations elsewhere, then perhaps it is the orographic gravity wave source that is enhanced. Another possibility would be the enhancement of the convection source, which is active considerably to the east and south of ALO. If that were the case, then we would predict that the Purple Crow lidar should also detect NLCs and these large vertical mesospheric waves.

[43] To further investigate the origin of these midlatitude NLCs will require more systematic, simultaneous, long-term observations with Rayleigh-scatter lidars at ALO and other locations. More sensitive lidars would improve the observations by obtaining data from higher altitudes, thereby minimizing uncertainties in the background and providing better time resolution. As demonstrated in this paper, significant additional information can be obtained by having a cluster of instrumentation providing more extensive observations. The Michelson Interferometer provided valuable, mesospheric temperature observations. It would be valuable if other instruments could provide mesospheric wind measurements, and if still others could provide temperature or density measurements from the upper troposphere into the mesosphere.

[44] **Acknowledgments.** This work was supported in part by Utah State University, NSF grant -0123145 and ATM-0531397, and a scholarship from the Rocky Mountain NASA Space Consortium. The data were acquired in part with support from Utah State University, several CEDAR grants from the Atmospheric Science Division of the NSF, and NASA OSS grant NAG5-5022. We greatly appreciate Dr. Maura Hagen for making the GSWM-00 tidal results available on the Web. We also greatly appreciate the helpful comments from two reviewers.

References

Baker, D. J., and A. T. Stair Jr. (1988), Rocket measurements of the altitude distributions of the hydroxyl airglow, *Phys. Scr.*, *37*, 611–622.

Burns, G. B., T. D. Kawahara, W. J. R. French, A. Nomura, and A. R. Klekociuk (2003), A comparison of hydroxyl rotational temperatures from Davis (69°S, 78°E) with sodium lidar temperatures from Syowa (69°S, 39°E), *Geophys. Res. Lett.*, *30*(1), 1025, doi:10.1029/2002GL016413.

Chandra, S., C. H. Jackman, E. L. Fleming, and J. M. Russell III (1997), The seasonal and long term changes in mesosphere water vapor, *Geophys. Res. Lett.*, *24*(6), 639–642, doi:10.1029/97GL00546.

Chu, X., C. Gardner, and R. G. Roble (2003), Lidar studies of interannual, seasonal, and diurnal variations of polar mesospheric clouds at the South Pole, *J. Geophys. Res.*, *108*(D8), 8447, doi:10.1029/2002JD002524.

Chu, X., G. J. Nott, P. J. Espy, C. S. Gardner, J. C. Diettrich, M. A. Clilverd, and M. J. Jarvis (2004), Lidar observations of polar mesospheric clouds at Rothera, Antartica (67.5°S, 68.0°W), *Geophys. Res. Lett.*, *31*, L02114, doi:10.1029/2003GL018638.

Collins, R. L., M. C. Kelley, M. J. Nicolls, C. Ramos, T. Hou, T. E. Stern, K. Mizutani, and T. Itabe (2003), Simultaneous lidar observations of a noctilucent cloud and an internal wave in the polar mesosphere, *J. Geophys. Res.*, *108*(D8), 8435, doi:10.1029/2002JD002427.

Espy, P. J., and J. Stegman (2002), Trends and variability of mesospheric temperature at high-latitudes, *Phys. Chem. Earth Part C*, *27*, 543–553.

Espy, P. J., R. Huppi, and A. Manson (1995), Large-scale, persistent latitude structures in the mesospheric temperature during ANLC-93, *Geophys. Res. Lett.*, *22*(20), 2801–2804, doi:10.1029/95GL03023.

Fiedler, J., G. Baumgarten, and G. von Cossart (2003), Noctilucent clouds above ALOMAR between 1997 and 2001: Occurrence and properties, *J. Geophys. Res.*, *108*(D8), 8453, doi:10.1029/2002JD002419.

Gadsden, M., and W. Schroder (1989), *Noctilucent Clouds*, 190 pp., Springer, New York.

Gardner, C. S. (1989), Sodium resonance fluorescence lidar applications in atmospheric science and astronomy, *Proc. IEEE*, *77*(3), 408–418.

Hagan, M., M. D. Burrage, J. M. Forbes, J. Hackney, W. J. Randel, and X. Zhang (1999), GSWM-98: Results for migrating solar tides, *J. Geophys. Res.*, *104*(A4), 6813–6827, doi:10.1029/1998JA900125.

Hagan, M., R. G. Roble, and J. Hackney (2001), Migrating thermospheric tides, *J. Geophys. Res.*, *106*(A7), 12,739–12,752, doi:10.1029/2000JA000344.

Hansen, G., M. Serwazi, and U. von Zahn (1989), First detection of a noctilucent cloud by lidar, *Geophys. Res. Lett.*, *16*(12), 1445–1448.

Herron, J. P. (2004), Mesospheric Temperature Climatology above Utah State University, M.S. thesis, Utah State University, Logan.

Hervig, M., R. E. Thompson, M. McHugh, L. L. Gordley, J. Russell, and M. E. Summers (2001), First confirmation that water ice is the primary component of polar mesospheric clouds, *Geophys. Res. Lett.*, *28*(6), 971–974, doi:10.1029/2000GL012104.

Langer, M., K. P. Müller, and K. H. Fricke (1995), Rayleigh lidar detection of aerosol echos from noctilucent cloud altitudes at the Arctic circle, *Geophys. Res. Lett.*, *22*(4), 381–384, doi:10.1029/94GL02903.

Liu, H.-L. (2000), Temperature changes due to gravity wave saturation, *J. Geophys. Res.*, *105*(D10), 12,329–12,336, doi:10.1029/2000JD900054.

Liu, H.-L., and M. E. Hagan (1998), Local heating/cooling of the mesosphere due to gravity wave and tidal coupling, *Geophys. Res. Lett.*, *25*(15), 2941–2944, doi:10.1029/98GL02153.

Liu, G., and G. G. Shepherd (2006), An empirical model for the altitude of the OH nightglow emission, *Geophys. Res. Lett.*, *33*, L09805, doi:10.1029/2005GL025297.

Liu, H.-L., M. E. Hagan, and R. G. Roble (2000), Local mean state changes due to gravity wave breaking modulated by the diurnal tide, *J. Geophys. Res.*, *105*(D10), 12,381–12,396, doi:10.1029/1999JD901163.

Lübken, F.-J. (1999), Thermal structure of the Arctic summer mesosphere, *J. Geophys. Res.*, *104*(D8), 9135–9149, doi:10.1029/1999JD900076.

Lübken, F.-J., K.-H. Fricke, and M. Langer (1996), Noctilucent clouds and the thermal structure near the Arctic mesopause in summer, *J. Geophys. Res.*, *101*(D5), 9489–9508, doi:10.1029/96JD00444.

Nedoluha, G. E., R. M. Bevilacqua, R. M. Gomez, B. C. Hicks, J. M. Russell, and B. J. Conner (2003), An evaluation of trends in middle atmospheric water vapor as measured by HALOE, WVMS, and POAM, *J. Geophys. Res.*, *108*(D13), 4391, doi:10.1029/2002JD003332.

She, C. Y., and R. P. Lowe (1998), Seasonal temperature variations in the mesopause region at mid-latitude: Comparison of lidar and hydroxyl

rotational temperatures using WINDII/UARS OH height profiles, *J. Atmos. Sol. Terr. Phys.*, *60*, 1573–1583.

She, C. Y., S. Chen, Z. Hu, J. Sherman, J. D. Vance, V. Vasoli, M. A. White, J. R. Yu, and D. A. Krueger (2000), Eight-year climatology of nocturnal temperature and sodium density in the mesopause region (80 to 105 km) over Fort Collins, CO (41°N, 105°W), *Geophys. Res. Lett.*, *27*(20), 3289–3292, doi:10.1029/2000GL003825.

She, C. Y., S. Chen, B. P. Williams, Z. Hu, and D. A. Krueger (2002), Tides in the mesopause region over Fort Collins, Colorado (41°N, 105°W) based on lidar temperature observations covering full diurnal cycles, *J. Geophys. Res.*, *107*(D18), 4350, doi:10.1029/2001JD001189.

States, R. J., and C. S. Gardner (2000), Thermal structure of the mesopause regioin (80–105 km) at 40°N latitude: Part II. Diurnal variations, *J. Atmos. Sci.*, *57*, 78–92.

Stebel, K., U. Blum, K.-H. Fricke, S. Kirkwood, N. J. Mitchell, and A. Osepain (2004), Joint radar/lidar observations of possible aerosol layers in the winter mesosphere, *J. Atmos. Sol. Terr. Phys.*, *66*, 957–970.

Thayer, J. P., N. Nielsen, and J. Jacobsen (1995), Noctilucent cloud observations over Greenland by a Rayleigh lidar, *Geophys. Res. Lett.*, *22*, 2961–2964, doi:10.1029/95GL02126.

Thomas, G. E. (1991), Mesospheric clouds and the physics of the mesopause region, *Rev. Geophys.*, *29*, 553–576.

Thomas, G. E. (1996), Is the polar mesosphere the miner's canary of global change?, *Adv. Space Res.*, *18*(3), 49–58.

Thomas, G. E. (1997), Introduction to special section: Noctilucent cloud workshop, *J. Geophys. Res.*, *102*(D2), 1957–1958, doi:10.1029/96JD03815.

Thomas, G. E. (2003), Are noctilucent clouds harbringers of global change in the middle atmosphere?, *Adv. Space Res.*, *32*(9), 1737–1746.

Thomas, G. E., and J. J. Olivero (1989), Climatology of polar mesospheric clouds: 2. Further analysis of Solar Mesosphere Explorer data, *J. Geophys. Res.*, *94*(D12), 14,673–14,681.

von Cossart, G., J. Fiedler, and U. von Zahn (1999), Size distribution of NLC particles as determined from 3-color observations of NLC by ground lidar, *Geophys. Res. Lett.*, *26*(11), 1513–1516, doi:10.1029/1999GL900226.

von Zahn, U., and U. Berger (2003), The altitude of noctilucent clouds: Groundbased observations and their interpretation through numerical modeling, in Proc. 16th ESA symposium on European rocket and balloon programmes and related research, edited by B. Warmbein, ESA SP-530, 295–301.

von Zahn, U., and W. Meyer (1989), Mesopause temperature in polar summer, *J. Geophys. Res.*, *94*(D12), 14,647–14,651.

von Zahn, U., K. H. Fricke, R. Gerndt, and T. Blix (1987), Mesospheric temperatures and the OH layer height as derived from ground-based lidar and OH* spectrometry, *J. Atmos. Terr. Phys.*, *49*, 863–869.

Walterscheid, R. L. (1981), Dynamical cooling induced by dissipating internal gravity waves, *Geophys. Res. Lett.*, *8*, 1235–1238.

Wickwar, V. B., T. D. Wilkerson, M. Hammond, and J. P. Herron (2001), Mesospheric temperature observations at the USU/CASS Atmospheric Lidar Observatory (ALO), in Remote Sensing of the Atmosphere, Environment, and Space, edited by U. N. Singh, T. Itabe, and N. Sugimoto *Proceedings of SPIE, 4153*, 272–284.

Wickwar, V. B., M. J. Taylor, J. P. Herron, and B. A. Martineau (2002), Visual and lidar observations of noctilucent clouds above Logan, Utah, at 41.7°N, *J. Geophys. Res.*, *107*(D7), 4054, doi:10.1029/2001JD001180.

P. J. Espy, Physical Science Division, British Antarctic Survey, Cambridge, UK.

J. P. Herron and V. B. Wickwar, Center for Atmospheric and Space Sciences, Utah State University, 4405 Old Main, Hill, Logan, UT 84322-4405, USA. (vincent.wickwar@usu.edu)

J. W. Meriwether, Department of Physics and Astronomy, Clemson University, Clemson, SC, USA.